Imaging of a vibrating object by Sideband Digital Holography

Fadwa Joud, Franck Laloë, Michael Atlan, Jean Hare, Michel Gross

▶ **To cite this version:**

HAL Id: hal-00321050

https://hal.archives-ouvertes.fr/hal-00321050v3

Submitted on 13 Mar 2009

Imaging a vibrating object by Sideband Digital Holography

F. Joud[1], F. Laloë[1], M. Atlan[2], J. Hare[1] and M. Gross[1].

[1] *Laboratoire Kastler Brossel – UMR 8552 École Normale Supérieure, UPMC, CNRS*
24 rue Lhomond ; 75231 Paris Cedex 05 ; France
[2] *Département de Biologie Cellulaire — Institut Jacques Monod, UMR 7592, CNRS, Univ.*
Paris 6 and 7 — 2 Place Jussieu ; 75251 Paris Cedex 05; France

gross@lkb.ens.fr

Abstract: We obtain quantitative measurements of the oscillation amplitude of vibrating objects by using sideband digital holography. The frequency sidebands on the light scattered by the object, shifted by n times the vibration frequency, are selectively detected by heterodyne holography, and images of the object are calculated for different orders n. Orders up to $n = 120$ have been observed, allowing the measurement of amplitudes of oscillation that are significantly larger than the optical wavelength. Using the positions of the zeros of intensity for each value of n, we reconstruct the shape of vibration the object.

References and links

1. R. Powell and K. Stetson, "Interferometric vibration analysis by wavefront reconstruction," J. Opt. Soc. Am **55**, 1593–1598 (1965). URL http://www.opticsinfobase.org/josa/abstract.cfm?URI=josa-55-12-1593.
2. P. Picart, J. Leval, D. Mounier, and S. Gougeon, "Time-averaged digital holography," Opt. Lett. **28**, 1900–1902 (2003). URL http://www.opticsinfobase.org/ol/abstract.cfm?URI=ol-28-20-1900.
3. F. Zhang, J. Valera, I. Yamaguchi, M. Yokota, and G. Mills, "Vibration Analysis by Phase Shifting Digital Holography," Opt. Rev. **11**, 297–299 (2004). URL http://dx.doi.org/10.1007/s10043-004-0297-7.
4. A. Asundi and V. Singh, "Time-averaged in-line digital holographic interferometry for vibration analysis," Appl. Opt. **45**, 2391–2395 (2006). URL http://www.opticsinfobase.org/ao/abstract.cfm?URI=ao-45-11-2391.
5. V. Singh, J. Miao, Z. Wang, G. Hegde, and A. Asundi, "Dynamic characterization of MEMS diaphragm using time averaged in-line digital holography," Opt. Commun. **280**, 285–290 (2007). URL http://dx.doi.org/10.1016/j.optcom.2007.08.030.
6. N. Demoli and D. Vukicevic, "Detection of hidden stationary deformations of vibrating surfaces by use of time-averaged digital holographic interferometry," Opt. Lett. **29**, 2423–2425 (2004). URL http://www.opticsinfobase.org/abstract.cfm?URI=ol-29-20-2423.
7. N. Demoli, "Real-time monitoring of vibration fringe patterns by optical reconstruction of digital holograms: mode beating detection," Opt. Express **14**, 2117–2122 (2006). URL http://www.opticsexpress.org/viewmedia.cfm?id=88786\&seq=0.
8. C. C. Aleksoff, "Temporally modulated holography," Appl. Opt. **10**, 1329–1341 (1971). URL http://www.opticsinfobase.org/abstract.cfm?URI=ao-10-6-1329.
9. F. LeClerc, L. Collot, and M. Gross, "Numerical Heterodyne Holography Using 2D Photo-Detector Arrays," Opt. Lett. **25**, 716–718 (2000). URL http://www.opticsinfobase.org/abstract.cfm?URI=ol-25-10-716.
10. F. Pinard, B. Laine, and H. Vach, "Musical quality assessment of clarinet reeds using optical holography," J. Acoust. Soc. Am. **113**, 1736–1742 (2003). URL http://dx.doi.org/10.1121/1.1543586.

11. M. Facchinetti, X. Boutillon, and A. Constantinescu, "Numerical and experimental modal analysis of the reed and pipe of a clarinet," J. Acoust. Soc. Am. **113**, 2874–2883 (2003). URL http://dx.doi.org/10.1121/1.1560212.
12. I. Yamaguchi and T. Zhang, "Phase-Shifting digital holography," Opt. Lett. **22**, 1268–1270 (1997). URL http://www.opticsinfobase.org/abstract.cfm?URI=ol-22-16-1268.
13. M. Atlan, M. Gross, and E. Absil, "Accurate phase-shifting digital interferometry," Opt. Lett. **32**, 1456–1458 (2007). URL http://www.opticsinfobase.org/abstract.cfm?URI=ol-32-11-1456.
14. E. Cuche, P. Marquet, and C. Depeursinge, "spatial filtering for zero-order and twin-image elimination in digital off-axis holography," Appl. Opt. **39**, 4070–4075 (2000). URL http://www.opticsinfobase.org/abstract.cfm?\&URI=ao-39-23-4070.
15. M. Gross and M. Atlan, "Digital holography with ultimate sensitivity," Opt. Lett. **32**, 909–911 (2007). URL http://www.opticsinfobase.org/abstract.cfm?URI=ol-32-8-909.
16. M. Gross, M. Atlan, and E. Absil, "Noise and aliases in off-axis and phase-shifting holography," Appl. Opt. **47**, 1757–1766 (2008). URL http://www.opticsinfobase.org/ao/abstract.cfm?URI=ao-47-11-1757
17. U. Schnars and W. Jüptner, "Direct recording of holograms by a CCD target and numerical reconstruction," Appl. Opt. **33**(2), 179–181 (1994). URL http://www.opticsinfobase.org/abstract.cfm?\&id=41154.

Holographic imaging is based on interferences between a signal optical field and a reference beam; it provides an accurate method to image the vibration of various objects. Powell and Stetson [1] have shown that the *time-averaged* hologram of an harmonically vibrating object involves the Bessel function $J_0(z)$, where z is the phase modulation amplitude. In the backscattering geometry, $z = 4\pi A/\lambda$ where A is the mechanical amplitude of vibration and λ the optical wavelength. Image reconstruction then provides a direct mapping of the amplitude A at various points of the object, in the form of dark fringes appearing around points where $J_0(z)$ is zero.

Picard et al. [2] have simplified the processing of the data by performing Time Averaged Digital Holography (TADH) with a CCD camera, leading to numerous recent developments [3, 4, 5, 6, 7]. Nevertheless, the quantitative measurement of vibration amplitudes remains limited to situations where fringes can be counted, which implies that the amplitudes of vibration must be relatively small; otherwise, it becomes difficult to count many narrow fringes, and even impossible when they are smaller than the optical resolution.

In this letter, we show how Sideband Digital Holography (SDH) can overcome the problem.
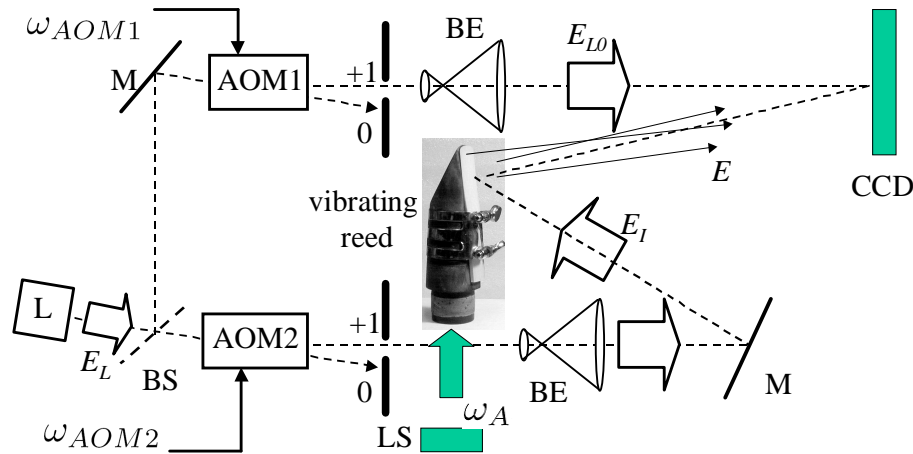

Fig. 1. Setup. L: main laser; AOM1, AOM2: acousto-optic modulators; M: mirror; BS: beam splitter; BE: beam expander; CCD: CCD camera; LS: loud-speaker exiting the clarinet reed at frequency $\omega_A/2\pi$.

Sideband holography was already demonstrated in 1971 by C.C. Aleksoff, in a pioneering experiment [8] where the reference beam was frequency-shifted by an ultrasonic diffraction cell; selecting a given frequency resulted in a selection of a given sideband of the signal backscattered by the object. The experiment was done with holographic plates. Here, we use digital heterodyne holography [9]; both reference and illumination laser beams are frequency shifted, and the selection of one sideband is obtained by a proper detuning of one of the beams followed by heterodyne detection on a CCD camera; this technique provides much more flexibility and leads to accurate quantitative measurements. As a demonstration, inspired by the work described in [10, 11] we perform an experiment where the vibrating object is the reed of a clarinet; in addition to the intrinsic interest of such an object, with its possible musical implications, a reed provides a test system that is particularly well adapted to our purposes, with typical vibration amplitudes of the order of 0.1 mm. We will see that, even with smaller amplitudes, there is no difficulty in obtaining holographic images corresponding to the nth sideband with n up to 100 or more.

The experimental setup is schematically shown in Fig. 1. A laser beam, with wavelength $\lambda \simeq 650$ nm (angular frequency ω_L) is split into a local oscillator beam (E_{LO}) and an illumination beam (E_I); their angular frequencies ω_{LO} and ω_I are tuned by using two acousto-optic modulators (Bragg cells with a selection of the first order diffraction beam) AOM1 and AOM2: $\omega_{LO} = \omega_L + \omega_{\text{AOM1}}$ and $\omega_I = \omega_L + \omega_{\text{AOM2}}$ where $\omega_{\text{AOM1,2}}/2\pi \simeq 80$ MHz. The clarinet reed is attached to a clarinet mouthpiece and its vibration is driven by a sound wave propagating inside the mouthpiece, as in playing conditions, but in our experiment the sound wave is created by a loudspeaker excited at frequency ω_A and has a lower intensity than inside a clarinet; no attempt has been made to reproduce the mechanical effect of the lip of the player. The excitation frequency is adjusted to be resonant with the first flexion mode (2143 Hz) of the reed. The phase of the field E backscattered by any element of the reed is then phase modulated at frequency ω_A, so that E can be expanded into carrier (E_0) and sideband components (E_n) as:

$$E(t) = \mathscr{E} e^{j\omega_I t} e^{jz\sin(\omega_A t)} = \sum_{n=-\infty}^{\infty} E_n(t) \tag{1}$$

$$E_n(t) = \mathscr{E} J_n(z) e^{j\omega_L t} e^{j(\omega_{\text{AOM2}} + n\omega_A)t} \tag{2}$$

where $\mathscr{E}$ is the complex field of the object in the absence of modulation, $z = 4\pi A/\lambda$ is the phase modulation amplitude, A the amplitude of vibration of the particular element, and J_n is the n-th order Bessel function of the first kind (with $J_{-n}(z) = (-1)^n J_n(z)$ for integer n and real z).

To selectively detect the nth sideband we use 4 phase shifting holography [12] and adjust the frequency ω_{AOM1} to fulfil the condition:

$$\omega_{\text{AOM2}} - \omega_{\text{AOM1}} - n\,\omega_A = \omega_{\text{CCD}}/4 \tag{3}$$

where ω_{CCD} is the CCD camera frame frequency and n is a (positive or negative) integer; the phase of the modulated signal is then shifted by 90° from one CCD image to the next [13]. The sideband complex hologram signal H_n provided by each pixel of the camera, proportional to the local sideband complex field, is obtained by 4-phase demodulation:

$$H_n = (I_0 - I_2) + j(I_1 - I_3)\,, \tag{4}$$

where $I_0, \cdots I_3$ are 4 consecutive intensity images digitally recorded by the CCD camera (Pike: Allied vision Technology Inc, 12 bits, $\omega_{\text{CCD}}/2\pi = 10$ Hz, exposure time 100 ms, 1340×1024 pixels). The LO beam is slightly angularly shifted ($\sim 1°$) with respect to the beam originating from the reed; in this way, the zero order and twin-image aliases [14] can be suppressed and an ultimate detection sensitivity can be reached [15, 16].
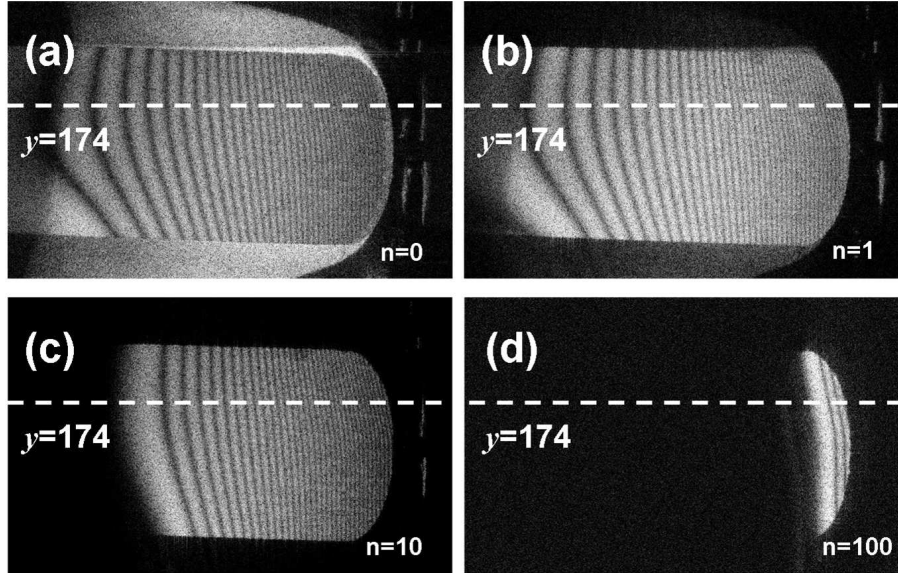
Fig. 2. Reconstructed holographic images of a clarinet reed vibrating at frequency $\omega_A/2\pi = 2143$ Hz perpendicularly to the plane of the figure. Figure (a) shows the carrier image obtained for $n = 0$; Fig. (b)-(d) show the frequency sideband images respectively for $n = 1$, $n = 10$, and $n = 100$. A logarithmic grey scale has been used.

From the complex holograms, the images of the reed are reconstructed by the standard convolution method [17]. To simplify the Fourier transform calculation, the 1340×1024 pixels data are truncated to 1024×1024. Because of the angular shift, the image of the reed lies in the upper side of the reconstruction grid. In figure 2, for pixels ranging from 200 to 1023 along the x axis and 0 to 511 on the y axis, we show the reconstructed images for different sideband orders n; only the square modulus of the complex signal is retained (the phase coming from $\mathscr{E}$ is ignored), so that we obtain intensity images, proportional to $|E_n|^2$ for each different sideband.

Figure 2(a) is obtained at the unshifted carrier frequency ($n = 0$). The left side of the reed is attached to the mouthpiece, and the amplitude of vibration is larger at the tip of the reed on the right side; in this region the fringes become closer and closer and difficult to count. The mouthpiece is also visible, but without fringes since it does not vibrate. Similar images of clarinet reeds have been obtained in [10, 11], with more conventional techniques and lower image quality. Figures 2(b)-2(d) show images obtained for three sideband frequencies. As expected, the non-vibrating mouthpiece is no longer visible. Figure 2(b) shows the $n = 1$ sideband image, with J_1 fringes that are slightly shifted with respect to those of J_0. Figure 2(c) shows the order $n = 10$ and (d) the order $n = 100$ (e). The left side region of the image remains dark because, in that region, the vibration amplitude is not sufficient to generate these sidebands, $J_n(z)$ being evanescent for $z < n$.

We have performed cuts of the reconstructed images signal $|E_n(x,y)|^2$ obtained for different sideband orders n along the horizontal line $y = 174$ (this value has been chosen because it corresponds to a region where the fringes are orthogonal to the y axis). To reduce the effect of speckle fluctuations, the intensity signal $|E_n(x, y = 174)|^2$ has been averaged over 20 pixels in the y direction ($y = 164\ldots184$). Moreover, since the illumination of the reed is not uniform, we have normalized the sideband signal by the reconstructed image intensity $|E|^2$ obtained at the carrier frequency ($n = 0$) without mechanical excitation of the reed (loud-speaker off). One
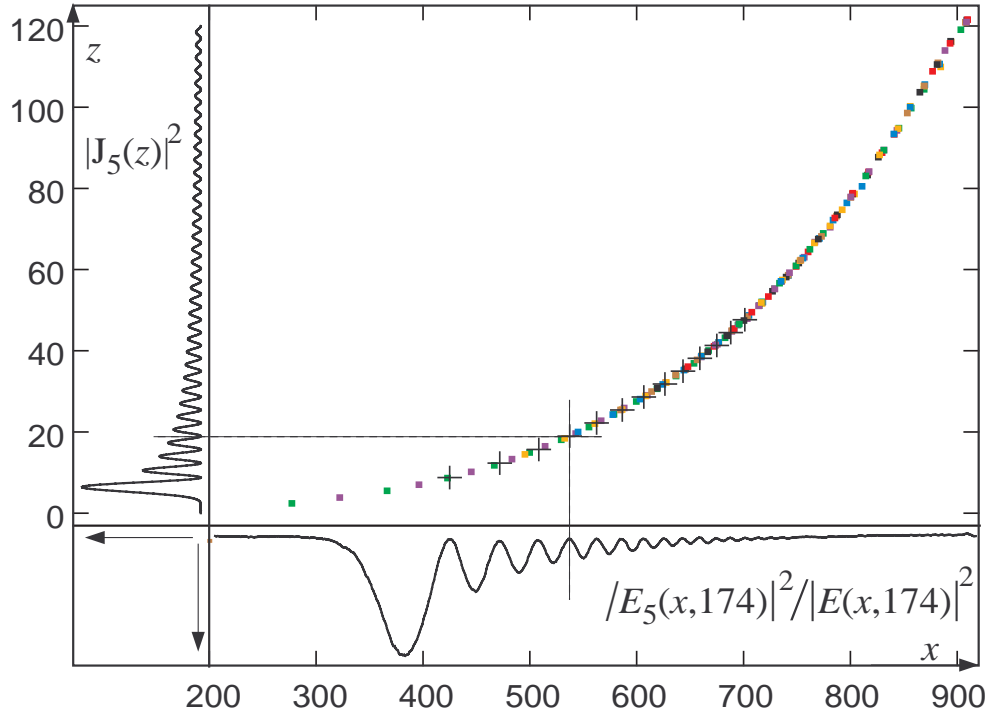
Fig. 3. A slice of the data along the $y = 174$ line is used in this figure; the x horizontal axis gives the pixel index (100 pixels correspond to 3.68 mm.), the vertical axis the phase modulation amplitude z. The lower part of the figure shows the normalized signal $|E_n(x)|^2/|E(x)|^2$ for a particular sideband order $n = 5$, with a downwards axis; the left part shows the corresponding square of the Bessel function $|J_5(z)|^2$ with a leftward axis. The zeroes of the two curves are put in correspondence, which provides the points in the central figure; a different color is used for each harmonic order $n = 0, 1, 5, 10...100$; the crosses correspond to $n = 5$. The juxtaposition of the points for all values of n gives an accurate representation of the amplitude of vibration A as a function of x.

example of the normalized signals $|E_n|^2/|E|^2$ along the cut is shown for $n = 5$, in the lower part of Fig. 3, with a downwards intensity axis. In this case, and for many other values of n, we have checked that the normalized curves vary as the square of Bessel functions, with a first fringe that moves to higher values when n increases (it occurs when $z \simeq n$ and the amplitude of vibrations increases with x). For instance, for $n = 0$, which corresponds to standard TADH, the variations of $|J_0(z)|^2$ show a large number of nodes and anti-nodes, with decreasing visibility for increasing x; above $x = 700$, the fringes are no longer visible. For $n = 20$, the first fringe, which corresponds to $z \simeq n = 20$, is located near $x \simeq 560$. Going to $n = 60$ pushes the first fringe to $x \simeq 755$, where the counting of fringes with TADH would no longer be possible. In a more general way, the first fringe on the nth sideband image provides a convenient marker for the region $z \simeq n$.

For a more precise treatment of the data, we use the position of the antinodes, which is insensitive to inhomogeneities of illumination; no normalization is then required. To build the central part of Fig. 3, a similar linear cut at $y = 174$ is processed, for the values $n = 0, 1, 5, 10, \ldots 100$. The x locations of the successive minima of the signal $|E_n(x)|^2$ are plotted against the zeros of the corresponding $|J_n(z)|^2$. To illustrate the way the points are obtained, we show in the left part

of the Fig. 3 the expected signal $|J_5(z)|^2$, to be compared to the signal in the lower part. For all observed sideband order n ranging from 0 to 100, all the points displayed on Fig. 3 fall on a well defined curve, which provides the vibration amplitude z as function of the location x. The excellent consistency of the overlapping data sets demonstrates the validity of expansions Eq. 1 for any order n. Therefore the figure provides a direct and accurate visualization of the map of the maximal elongations of the reed, from the left part clamped on the mouthpiece to the tip on the right; here, the maximum amplitude is $z \simeq 120$ radians, corresponding to $A \simeq 6.2\ \mu$m.

To conclude, recording separately different sideband Fourier components of the light back-scattered by a vibrating object gives access to a large amount of information; this can be used to remove ambiguities and inaccuracies in measurements of large modulation amplitude. Using large sideband order n actually makes the calibration of the vibration amplitude z straightfor-ward: the first fringe of a high order image can be used as a marker. This marker is easy to locate since it corresponds to a fast transition from zero signal, and moreover is brighter and broader. Performing sideband holography with many orders n gives a direct and accurate ac-cess to the shape of the vibration amplitude and its position dependence. Figure 3 shows only a representation of a slice of the data along one given axis, but more information is available if one changes the value of y or chooses another direction, for instance parallel to y to accurately map the transverse variations of the amplitude A. Sideband digital holography therefore opens up a variety of new possibilities in holography.